ELSEVIER

Applied Ocean Research 22 (2000) 267–280

Applied Ocean Research

www.elsevier.com/locate/apor

A causal transient water wave diffraction formulation

C.J. Damaren*

Institute for Aerospace Studies, University of Toronto, 4925 Dufferin Street, Toronto, Ont., Canada M3H 5T6

Received 12 February 2000; revised 11 July 2000; accepted 20 July 2000

Abstract

The frequency-domain description of the potential function corresponding to a sinusoidal progressing wave can form the basis for describing an arbitrary incident wave field in linearized free-surface hydrodynamics. Fourier techniques make it possible to relate the incident sea state to the resulting hydrodynamic forces on a floating body. This paper develops a rational description in the frequency domain for the corresponding dynamical system which can then be realized in the time domain as a system of constant-coefficient differential equations driven by incident wave height at a datum and whose output is the Froude–Krylov force. This is made possible by showing that the time-domain version of the potential for a sinusoidal progressing wave satisfies a fourth-order time-varying ordinary differential equation (ODE) analogous to that satisfied by the three-dimensional time-domain source function. Laplace transformation of this ODE followed by bilinear transformation supplies the analytical basis for generating the rational approximation. Various causality issues associated with the diffraction forces are neatly handled by the approach presented here.

Keywords: Water wave diffraction; Froude–Krylov forces; Transient hydrodynamics

1. Introduction

When one considers the small motions of a floating body in the presence of small amplitude incident waves, the hydrodynamic pressure forces can be taken to arise from three sources: the incident wave field, the scattered field produced by the presence of the body (collectively referred to as the diffraction field), and the motion of the body (radiation field). For purposes of modeling the floating body, it is natural to consider the dynamical systems which produce these forces under the action of appropriate inputs. For the radiation forces, the inputs may be taken as the (generalized) body velocities whereas for the diffraction problem it is natural to consider the amplitude of the free-surface elevation at some reference location. In the sequel, the corresponding dynamical systems are referred to as the radiation (mapping) impedance and the diffraction mapping.

For the linearized version of what is ultimately a time-invariant problem, these dynamical systems can be realized by time-invariant convolution integrals which can be interpreted as inverse Fourier transforms of the product of the Fourier transforms of the impulse response and the corresponding input. From linear system theory, it is known that the Fourier transform of the impulse response of a linear time-invariant (LTI) system is equivalent to the complex amplitude of steady-state sinusoidal responses. Hence, in principle, transient solutions for the radiation and diffraction forces can be obtained using the inverse Fourier transform in conjunction with the solution of the corresponding steady-state time-harmonic problem at many frequencies. The connection between the time- and frequency-domain formulations of linear water wave problems was noted by Cummins [1] and Wehausen [2].

Finite-dimensional approximations of LTI systems can also be written in state-space form which is no more than a nonhomogeneous system of first-order constant-coefficient ordinary differential equations (ODEs). The goal of the present paper is to obtain a state-space representation for the diffraction mapping. Yu and Falnes [3] were motivated by the same goal and used curve-fitting techniques that ultimately required a description for the complex force amplitudes at many frequencies. They ‘fitted’ the state-space system using time-domain impulse response data obtained using numerical inverse Fourier transforms of the frequency-domain information.

Falnes [4] has pointed out that the diffraction mapping is ultimately noncausal (i.e. the diffraction forces start before the datum wave height ‘begins’). Yu and Falnes demonstrate that the diffraction mapping can be made approximately causal by shifting the spatial datum for the incident field up-wave of the body or by time shifting the

* Tel.: +1-416-667-7704; fax: +1-416-667-7799.
E-mail address: cjd@sdr.utias.utoronto.ca (C.J. Damaren).

0141-1187/00/$ - see front matter
PII: S0141-1187(00)00020-1

impulse response, effectively delaying the force output relative to the wave input. Damaren [5] also realized the diffraction mapping by a state-space system but the fitting was conducted in the frequency domain using appropriate rational functions. The key idea was the recognition that linear, constant-coefficient ODEs in the time domain correspond to rational dependence on the frequency variable in the frequency domain. Causal approximations were obtained by forcing the rational descriptions to have poles in the left-half of the complex plane.

Many authors have been concerned with the transient motion of floating bodies but the majority of this work has treated the radiation problem. We mention Yeung [6], Newman [7], Beck and Liapis [8], and Pot and Jami [9], all of whom used the time-domain source function in conjunction with the transient version of a Fredholm integral equation. Analogous calculations for the diffraction problem (for bodies with forward speed) have been presented by Beck [10] and Korsmeyer and Bingham [11]. A rational approximation for the three-dimensional (3D) (frequency-domain) Green's function was obtained by Damaren [12] and used to obtain a rational description for the radiation impedance. This was obtained using the fourth-order time-varying ODE which Clément [13] has shown is satisfied by the time-domain source function. These calculations are analytical in character and permit a state-space description of the transient radiation problem without solving the frequency-domain problem at several frequencies. This paper presents the corresponding treatment of the diffraction problem.

The main result that is presented and exploited here is the fourth-order ODE satisfied by a family of two-dimensional (2D) "source" functions. These include the 2D (time-domain) Green's function and the time-domain potential corresponding to an impulsive change in free-surface elevation. The Fourier transform of the latter is the usual potential function attributed to a sinusoidal plane progressive wave. With this ODE in hand, the analytical techniques presented by Damaren [12] are used to develop rational approximations for the frequency-domain quantities. Multiplication of these "source" functions by an "input" function in the frequency domain yields convolution operators in the time domain whose action can be obtained as the "output" of a system of linear constant-coefficient ODEs corresponding to the rational approximation.

The main application treated here is the time-domain calculation of the transient Froude–Krylov force. In this case, the "input" referred to above is the transient incident wave height at a suitable datum and the "output" is the generalized exciting (Froude–Krylov) force in a general degree of freedom. The computational load required to generate the state-space model relating the two is on the order of that required to solve the frequency-domain problem at one frequency. Furthermore, being a standard state-space model, it is readily combined with structural and rigid-body motion equations and the corresponding treatment for the radiation problem developed in Ref. [12]. It is the explicit nature of the model which is most important and makes it suitable for applications such as control system design.

As mentioned above, the diffraction mapping is noncausal which in the time domain manifests itself as an impulse response that is nonzero for negative values of time and in the frequency domain by poles in the right-half of the complex plane. In physical terms, a wave height time history that begins at $t = 0$ generates exciting forces that begin before $t = 0$; this is obviously problematic in a simulation environment. Causal approximations can be obtained in a number of ways. Here, it is argued that truncation of the anticausal part of the potential function corresponding to an impulsive wave height in the time domain is a reasonable way to proceed and is easily accomplished using the methodology presented here. In the (complex) frequency domain, this corresponds to neglecting those contributions to a partial fraction expansion whose poles lie in the right-half of the complex plane. It is an optimal causal approximation to the incident wave potential function in the sense that it minimizes the energy of the potential error (the difference between the true potential and its causal approximation) corresponding to an impulsive change in wave height at the datum. Our primary interest here is the transient description of the Froude–Krylov force given the incident wave. However, the scattering component of the total diffraction force will also be described using the transient form of the Haskind relations.

2. The water wave diffraction problem

Consider the small motions of a floating body $\mathscr{B}$ in the presence of an incoming wave field. The free surface elevation in the absence of the body is described by $\zeta_I(\mathbf{r}, t)$ where $\mathbf{r} = [x\ y\ z]^T$. The z-axis is vertically upwards and the origin of the coordinate system lies in the undisturbed free surface and corresponds to a datum for describing the incident field: $\zeta_0(t) \triangleq \zeta_I(\mathbf{0}, t)$. The motions of the body are described by $\mathbf{w}(\mathbf{r}, t) = [w_1\ w_2\ w_3]^T$ and

$$\mathbf{w}(\mathbf{r}, t) = \sum_{\alpha=1}^{N} \Gamma_\alpha(\mathbf{r}) u_\alpha(t) \tag{1}$$

where Γ_α are shape functions which include the six rigid-body motions.

The wetted surface of $\mathscr{B}$ is denoted by S and $\mathbf{n}(\mathbf{r})$ is the outward normal to S. If $p(\mathbf{r},t)$ is the fluid pressure, then the fluid pressure force in "mode" α is given by

$$f_\alpha(t) = -\int_S p n_\alpha \, dS, \qquad n_\alpha(\mathbf{r}) \triangleq \mathbf{n}^T \Gamma_\alpha. \tag{2}$$

Given the assumptions that the fluid medium is incompressible, of constant density, inviscid, and irrotational, the fluid mechanics can be described by the velocity potential $\Phi(\mathbf{r}, t)$. If the ocean is modeled as infinitely deep and of infinite

extent, the velocity potential satisfies

$$\nabla^2\Phi = 0, \quad \mathbf{r} \in V, \qquad \frac{\partial^2\Phi}{\partial t^2} = -g\frac{\partial\Phi}{\partial z}, \quad \mathbf{r} \in F,$$
$$\lim_{z\to-\infty}\frac{\partial\Phi}{\partial z} = 0, \tag{3}$$

where $F = \{z = 0 \backslash \mathscr{B}\}$ denotes the free surface and g is the acceleration due to gravity.

The standard decomposition of Φ is used here

$$\Phi = \Phi_I + \Phi_S + \Phi_R, \qquad \Phi_R = \sum_{\alpha=1}^{N} \phi_{R\alpha} * \dot{u}_\alpha \tag{4}$$

where Φ_I, Φ_S, and Φ_R are respectively, the incident, scattered, and radiated fields, and $(*)$ denotes temporal convolution. Each function is a solution of the boundary value problem in Eq. (3) and

$$\frac{\partial\Phi_I}{\partial z}(\mathbf{r},t) = \frac{\partial\zeta_I}{\partial t}, \quad \mathbf{r} \in F, \tag{5}$$

$$\frac{\partial\Phi_S}{\partial n}(\mathbf{r},t) = -\frac{\partial\Phi_I}{\partial n}(\mathbf{r},t), \quad \mathbf{r} \in S, \tag{6}$$

$$\frac{\partial\Phi_{R\alpha}}{\partial n}(\mathbf{r},t) = n_\alpha(\mathbf{r})\delta(t), \quad \mathbf{r} \in S. \tag{7}$$

In addition, the scattered and radiated fields satisfy certain regularity conditions as $r \triangleq \sqrt{x^2+y^2} \to \infty$.

The radiation problem has been treated in the spirit of this paper elsewhere. Therefore, our attention is restricted to the diffraction field which is identified with $\Phi_D \triangleq \Phi_I + \Phi_S$. The linearized form of the Bernoulli relation implies that the corresponding hydrodynamical contribution to Eq. (2) is given by

$$f_{D\alpha}(t) = f_{I\alpha}(t) + f_{S\alpha}(t), \tag{8}$$

$$f_{I\alpha}(t) = \rho\int_S \frac{\partial\Phi_I}{\partial t} n_\alpha \, dS, \tag{9}$$

$$f_{S\alpha}(t) = \rho\int_S \frac{\partial\Phi_S}{\partial t} n_\alpha \, dS, \tag{10}$$

where ρ is the fluid density. The contribution $f_{I\alpha}(t)$ is the Froude–Krylov force.

The primary goal of the paper is to obtain an explicit representation for the dynamical system relating $\zeta_0(t)$ to $f_{I\alpha}(t)$. To this end, the Laplace transform of ζ_0 is defined by

$$\mathscr{L}\{\zeta_0(t)\} = \tilde{\zeta}_0(s) = \int_0^\infty e^{-st}\zeta_0(t)\,dt, \qquad Re\{s\} > 0,$$

a notation used throughout. The corresponding Fourier transform will also be used and is designated $\mathscr{F}\{\zeta(t)\} = \tilde{\zeta}_0(j\omega)$, and in the absence of arguments, say $\tilde{\zeta}_0$, the Fourier transform is intended. The inverse Fourier transform is

$$\zeta_0(t) = \mathscr{F}^{-1}\{\tilde{\zeta}_0(j\omega)\} = \frac{1}{2\pi}\int_{-\infty}^{\infty}\tilde{\zeta}_0(j\omega)e^{j\omega t}\,d\omega. \tag{11}$$

The velocity potential corresponding to ζ_0 is given by

$$\Phi_I(\mathbf{r},t) = \frac{1}{2\pi}\int_{-\infty}^{\infty}\tilde{\phi}_I(\mathbf{r},j\omega)\tilde{\zeta}_0(j\omega)e^{j\omega t}\,d\omega \tag{12}$$

where

$$\tilde{\phi}_I(\mathbf{r},j\omega) = \frac{jg}{\omega}e^{kz-jk'x} \tag{13}$$

with

$$k = \omega^2/g, \qquad k' = k\,\mathrm{sgn}(\omega).$$

The potential in Eq. (13) when multiplied by $e^{j\omega t}$ is recognized as that corresponding to a plane progressing wave in the positive x-direction with time dependence of this form; hence, Eq. (12) represents a superposition of such waves. It is readily verified that

$$\zeta_I(x,y,t) = -\frac{1}{g}\frac{\partial\Phi_I}{\partial t}\bigg|_{z=0} = \frac{1}{2\pi}\int_{-\infty}^{\infty}\tilde{\zeta}_0(j\omega)e^{-jk'x}\,e^{j\omega t}\,d\omega \tag{14}$$

which yields Eq. (11) upon setting $x = 0$.

Taking the inverse Fourier transform of Eq. (13) yields the required transient form:

$$\begin{aligned}\phi_I(\mathbf{r},t) &= \frac{jg}{2\pi}\int_{-\infty}^{\infty}\frac{1}{\omega}e^{kz-jk'x+j\omega t}\,d\omega \\ &= Re\left\{\frac{jg}{\pi}\int_0^\infty\frac{1}{\omega}e^{kz-jkx+j\omega t}\,d\omega\right\} \\ &= \frac{g}{\pi}\int_0^\infty\frac{1}{\omega}e^{kz}\sin(kx-\omega t)\,d\omega \\ &= \frac{g}{\pi}\int_0^\infty\frac{1}{\omega}e^{kz}\sin kx\cos\omega t\,d\omega \\ &\quad - \frac{g}{\pi}\int_0^\infty\frac{1}{\omega}e^{kz}\cos kx\sin\omega t\,d\omega \\ &= \frac{g}{2\pi}\int_0^\infty\frac{1}{k}e^{kz}(\sin kx\cos\sqrt{kg}t - \cos kx\sin\sqrt{kg}t)\,dk.\end{aligned} \tag{15}$$

Physically, ϕ_I corresponds to the potential resulting from an impulsive change in the free surface elevation at the origin, $\zeta_0(t) = \delta(t)$. As mentioned in the introduction, $\phi_I(\mathbf{r},t) \neq 0$ for $t < 0$ and hence is noncausal. In other words, the wave field required to produce the impulsive wave at the origin must start before then. This is an artifact of a description which is restricted to waves propagating in a single direction.

Given the form of Eq. (12), the general expression for the time-domain potential is

$$\Phi_I(\mathbf{r},t) = \phi_I * \zeta_0 = \int_{-\infty}^{\infty}\phi_I(\mathbf{r},t-\tau)\zeta_0(\tau)\,d\tau \tag{16}$$

which can be substituted into Eq. (9) to yield the Froude–Krylov force. Taking Fourier transforms in Eq. (9) gives the

frequency-domain description for these exciting forces:

$$\tilde{f}_{I\alpha} = \tilde{H}_{I\alpha}(j\omega)\tilde{\zeta}_0, \qquad \tilde{H}_{I\alpha}(j\omega) \triangleq j\omega\rho\int_S (\tilde{\phi}_I n_\alpha)\,\mathrm{d}S \tag{17}$$

and a similar construction applies to $\tilde{f}_{D\alpha}$. The goal here is a formulation in the frequency domain which yields an approximation to $\tilde{H}_{I\alpha}$ exhibiting rational dependence on frequency. This allows the diffraction mapping to be realized as a linear system of constant-coefficient differential equations forced by the reference wave motion $\zeta_0(t)$. In our previous work [5], this was accomplished by fitting values of $\tilde{H}_{I\alpha}(j\omega)$ with rational functions of s that were analytic in the right half-plane. This required solving the frequency-domain boundary value problem at many frequencies for each mode n_α.

In this paper, the rational description will be constructed analytically with causality as an essential feature of the development. Since $f_{I\alpha}(t) = H_{I\alpha} * \zeta_0(t)$ must be linear time-invariant, a finite-dimensional approximation must be of the state-space form

$$\dot{\mathbf{x}}_I(t) = \mathbf{A}_I\mathbf{x}_I + \mathbf{B}_I\zeta_0(t) \tag{18}$$

$$f_{I\alpha}(t) = \mathbf{C}_I\mathbf{x}_I + \mathbf{D}_I\zeta_0(t) \tag{19}$$

where $\mathbf{x}_I(t)$ is the n-dimensional state vector and $\{\mathbf{A}_I, \mathbf{B}_I, \mathbf{C}_I, \mathbf{D}_I\}$ are constant matrices of appropriate dimension. Taking Laplace transforms in to Eqs. (18) and (19) yields

$$\tilde{f}_{I\alpha}(s) = [\mathbf{C}_I(s\mathbf{1} - \mathbf{A}_I)^{-1}\mathbf{B}_I + \mathbf{D}_I]\tilde{\zeta}_0(s). \tag{20}$$

By obtaining $\tilde{H}_{I\alpha}(s)$ in this form, the transient description in Eqs. (18) and (19) will follow immediately.

3. Causal approximation

Analogous to Eq. (16) for the incident potential, Eq. (17) yields the convolution

$$f_{I\alpha}(t) = \int_{-\infty}^{\infty} H_{I\alpha}(t-\tau)\zeta_0(\tau)\,\mathrm{d}\tau \tag{21}$$

or in the frequency domain $\tilde{f}_{I\alpha}(s) = \tilde{H}_{I\alpha}(s)\tilde{\zeta}_0(s)$ where, in this section, in-general, $\tilde{(\cdot)}(s)$ denotes the double-sided Laplace transform. Let us define the following spaces of time-domain functions:

$$\mathscr{L}_2(-\infty,\infty) = \left\{h(t)\middle|\int_{-\infty}^{\infty} h^2(t)\,\mathrm{d}t < \infty\right\},$$

$$\mathscr{L}_2[0,\infty) = \left\{h_+(t)\middle|\int_{0}^{\infty} h_+^2(t)\,\mathrm{d}t < \infty\right\},$$

$$\mathscr{L}_2(-\infty,0] = \left\{h_-(t)\middle|\int_{-\infty}^{0} h_-^2(t)\,\mathrm{d}t < \infty\right\}.$$

Important for rigorously defining the process of causal approximation are the Hardy spaces. $\mathscr{H}_2$ are the functions $\tilde{h}(s)$ which are analytic in $Re\{s\} > 0$ and satisfy the condition

$$\sup_{\sigma>0}\int_{-\infty}^{\infty} |\tilde{h}(\sigma + j\omega)|^2\,\mathrm{d}\omega < \infty.$$

$\mathscr{H}_2^\perp$ are the functions $\tilde{h}(s)$ which are analytic in $Re\{s\} < 0$ and satisfy the condition

$$\sup_{\sigma<0}\int_{-\infty}^{\infty} |\tilde{h}(\sigma + j\omega)|^2\,\mathrm{d}\omega < \infty.$$

The space $\mathscr{L}_2(-j\infty, j\infty)$ are those functions $\tilde{h}(s)$ for which

$$\|\tilde{h}\|_2 = \sqrt{\frac{1}{2\pi}\int_{-\infty}^{\infty} |\tilde{h}(j\omega)|^2\,\mathrm{d}\omega} < \infty$$

and $\mathscr{L}_\infty(-j\infty, j\infty)$ are those functions $\tilde{h}(s)$ for which

$$\|\tilde{h}\|_\infty = \sup_{\omega\in R} |h(j\omega)| < \infty.$$

We have the following decompositions: $\mathscr{L}_2(-\infty,\infty) = \mathscr{L}_2(-\infty,0] \oplus \mathscr{L}_2[0,\infty)$ and $\mathscr{L}_2(-j\infty, j\infty) = \mathscr{H}_2 \oplus \mathscr{H}_2^\perp$. The functions in $\mathscr{H}_2$ are simply the Laplace transforms of the time signals in $L_2[0,\infty)$ and those in $\mathscr{H}_2^\perp$ are the Laplace transforms of the time signals in $L_2(-\infty,0]$.

Lastly, $\mathscr{H}_\infty$ contains the functions $\tilde{h}(s)$ which are analytic and bounded in $Re(s) > 0$. It consists of the Laplace transforms of those functions $h(t)$ which map $\mathscr{L}_2[0,\infty)$ onto $\mathscr{L}_2[0,\infty]$ via the convolution operation or, alternatively, map $\mathscr{H}_2$ onto $\mathscr{H}_2$ via multiplication. They correspond to causal systems and necessarily satisfy $h(t) = 0$, $t < 0$. $\mathscr{H}_2$ may be identified with the Laplace transforms of those $h(t)$ with finite energy which vanish for $t < 0$. The rational functions $\tilde{h}(s) \in \mathscr{H}_\infty$ for which $\lim_{s\to\infty}\tilde{h}(s) = 0$ are identical to the rational functions in $\mathscr{H}_2$.

Given a system $\tilde{H}_{I\alpha}(s) \in \mathscr{L}_\infty(-j\infty, j\infty) \cap \mathscr{L}_2(-j\infty, j\infty)$, there are two possibilities for defining a causal approximation: (i) find $\tilde{h}(s) \in \mathscr{H}_\infty$ to minimize $\|\tilde{H}_{I\alpha}(s) - \tilde{h}(s)\|_\infty$, or (ii) find $\tilde{h}(s) \in \mathscr{H}_2$ to minimize $\|\tilde{H}_{I\alpha}(s) - \tilde{h}(s)\|_2$. The first of these is the Nehari problem for which the optimal approximation is relatively difficult to determine and typically satisfies $\lim_{s\to\infty}\tilde{h}(s) \neq 0$ although $\tilde{H}_{I\alpha}(s) \to 0$ as $s \to \infty$. On the other hand, if $H_{I\alpha}(t) = h_+(t) + h_-(t)$ with $h_+(t) \in \mathscr{L}_2[0,\infty)$ and $h_-(t) \in \mathscr{L}_2(-\infty,0]$, then the optimal $\mathscr{H}_2$-approximation is $\tilde{h}(s) = \tilde{h}_+(s) = \mathscr{L}\{h_+(t)\}$, which effectively minimizes the energy of the impulse response error. It is readily computed by truncating the anticausal part $[h_-(t)]$ of $H_{I\alpha}(t)$ and can be accomplished by multiplying the right-hand side of Eq. (15) by $H(t)$, the Heaviside step function, and using its transform in Eq. (17).

4. An ODE for the impulsive wave height potential

In this section, Clément's treatment of the 3D source function is extended to certain cases of interest in the 2D case. In particular, the 2D source function and the potential

Table 1
Initial conditions for the fourth-order ODE

$F(\mu,\ell,\tau)$	ℓ	B_0	B_1	B_2	B_3
$\sqrt{r_1/g}\bar{\mathcal{G}}(\mathbf{r},\boldsymbol{\xi},t)$	$-\frac{1}{2}$	0	μ	0	$1-2\mu^2$
$\sqrt{r_1^3/g}\partial\bar{\mathcal{G}}/\partial x$	$\frac{1}{2}$	0	$-2\mu\sqrt{1-\mu^2}$	0	$-2\sqrt{1-\mu^2}(1-4\mu^2)$
$\sqrt{r_1^3/g}\partial\bar{\mathcal{G}}/\partial z$	$\frac{1}{2}$	0	$2\mu^2-1$	0	$2\mu(3-4\mu^2)$
$(2\pi/g)\phi_1(\mathbf{r},t)$	-1	$\tan^{-1}[\sqrt{1-\mu^2}/\mu]$	$-\sqrt{\pi(1+\mu)/2}$	$-\sqrt{1-\mu^2}$	$-\sqrt{\pi(1+\mu)/2}(1-2\mu)/2$
$(2\pi r_1/g)\partial\phi_1/\partial x$	0	μ	$\sqrt{\pi(1-\mu)/2}(1+2\mu)/2$	$1-2\mu^2$	$\sqrt{9\pi/32(1-\mu)}[4\mu^3-2\mu^2-3\mu+1]$
$(2\pi r_1/g)\partial\phi_1/\partial z$	0	$\sqrt{1-\mu^2}$	$\sqrt{\pi(1+\mu)/2}(1-2\mu)/2$	$-2\mu\sqrt{1-\mu^2}$	$\sqrt{9\pi/32(1+\mu)}[4\mu^3-2\mu^2-3\mu-1]$

$\mathbf{r}=[x\ z]^{\mathrm{T}}$; $\boldsymbol{\xi}=[\xi\ \zeta]^{\mathrm{T}}$(= 0 for ϕ_1), $r_1=\sqrt{(x-\xi)^2+(z+\zeta)^2}$, $\tau=t\sqrt{g/r_1}$, $\mu=-(z+\zeta)/r_1$

corresponding to an impulsive wave height can be treated. The basic result is covered by the following lemma:

Lemma. *The functions*

$$F(\mu,\ell,\tau)=\int_0^\infty \lambda^\ell \mathrm{e}^{-\mu\lambda}\left\{\begin{matrix}\cos(\sqrt{1-\mu^2}\lambda)\\ \sin(\sqrt{1-\mu^2}\lambda)\end{matrix}\right\}\left\{\begin{matrix}\cos(\sqrt{\lambda}\tau)\\ \sin(\sqrt{\lambda}\tau)\end{matrix}\right\}\mathrm{d}\lambda \tag{22}$$

satisfy the ordinary differential equation

$$A_4\frac{\partial^4 F}{\partial\tau^4}+A_3\tau\frac{\partial^3 F}{\partial\tau^3}+(A_2+\bar{A}_2\tau^2)\frac{\partial^2 F}{\partial\tau^2}+A_1\tau\frac{\partial F}{\partial\tau}+A_0F=0 \tag{23}$$

where the coefficients are given by

$$A_4=1,\qquad A_3=\mu,\qquad A_2=2(\ell+2)\mu,\qquad \bar{A}_2=\tfrac{1}{4},$$
$$A_1=\ell+\tfrac{7}{4},\qquad A_0=(\ell+1)(\ell+2). \tag{24}$$

The proof is given in Appendix A and extends the result of Clément which applied to a function of the form in Eq. (22) but the trigonomentric functions $\cos(\sqrt{1-\mu^2}\lambda)$ and $\sin(\sqrt{1-\mu^2}\lambda)$ were replaced with the Bessel functions $J_\nu(\sqrt{1-\mu^2}\lambda)$. In the sequel, the boundary conditions required to completely specify $F(\mu,\ell,t)$ are denoted by

$$F(\mu,\ell,0)=B_0,\qquad \frac{\partial F}{\partial\tau}(\mu,\ell,0)=B_1,$$
$$\frac{\partial^2 F}{\partial\tau^2}(\mu,\ell,0)=B_2,\qquad \frac{\partial^3 F}{\partial\tau^3}(\mu,\ell,0)=B_3. \tag{25}$$

4.1. The 2D Green's function

Before considering the impulsive wave height potential, recall that the 2D Green's function in the frequency domain [14] can be written as

$$\bar{\mathcal{G}}(\mathbf{r},\boldsymbol{\xi};j\omega)=\triangleq \log\left(\frac{r_\xi}{r_1}\right)-2\int_0^\infty \frac{1}{\kappa-k}\mathrm{e}^{\kappa(z+\zeta)}\times\cos[\kappa(x-\xi)]\,\mathrm{d}\kappa \tag{26}$$

where $r_\xi^2=(x-\xi)^2+(z-\zeta)^2$ and $r_1^2=(x-\xi)^2+(z+\zeta)^2$. The integration in Eq. (26) passes above the pole at $\kappa=k$ in order to satisfy the radiation condition. This describes the complex amplitude of the potential field arising from an oscillating source with frequency $\omega=\sqrt{kg}$ at $\mathbf{r}=\boldsymbol{\xi}=[\xi\ \eta\ \zeta]^{\mathrm{T}}$.

The transient form of this function is obtained using the inverse Fourier transform:

$$\mathcal{G}(\mathbf{r},\boldsymbol{\xi};t)=\log\left(\frac{r_\xi}{r_1}\right)\delta(t)-2\bar{\mathcal{G}}(\mathbf{r},\boldsymbol{\xi};t),$$
$$\bar{\mathcal{G}}(\mathbf{r},\boldsymbol{\xi};t)=\int_0^\infty \mathrm{e}^{\kappa(z+\zeta)}\cos[\kappa(x-\xi)]\sqrt{\frac{g}{\kappa}}\sin(t\sqrt{g\kappa})\,\mathrm{d}\kappa\,H(t). \tag{27}$$

Here, $\delta(t)$ is the Dirac delta function and $H(t)$ is the Heaviside step function. This describes the time-varying potential field arising from a source with strength $\delta(t)$ at $\mathbf{r}=\boldsymbol{\xi}$.

By defining

$$\lambda=\kappa r_1,\qquad \mu=\frac{-(z+\zeta)}{r_1},\qquad \tau=\sqrt{\frac{g}{r_1}}t, \tag{28}$$

we have $\bar{\mathcal{G}}(\mathbf{r},\boldsymbol{\xi};\tau\sqrt{r_1/g})=\sqrt{g/r_1}F(\mu,\ell,\tau)$ with $\ell=-1/2$ assuming that the $\cos(\sqrt{1-\mu^2}\lambda)\sin(\sqrt{\lambda}\tau)$ combination is selected in Eq. (22). The corresponding initial conditions for F and its first three temporal derivatives can be determined by evaluating Eq. (22) and its derivatives at $\tau=0$ and recognizing that the ensuing integrals have the form of Laplace transforms (in μ). Hence, we obtain

$$A_4=1,\qquad A_3=\mu,\qquad A_2=4\mu,\qquad \bar{A}_2=\tfrac{1}{4},$$
$$A_1=\tfrac{7}{4},\qquad A_0=\tfrac{9}{4},\qquad B_0=0,\qquad B_1=\mu,$$
$$B_2=0,\qquad B_3=1-2\mu^2.$$

Note that the nondimensionalized function F depends (spatially) only on μ. The corresponding expressions for the A_i, B_i when

$$F = \sqrt{r_1^3/g}\partial\bar{G}/\partial x$$

or

$$F = \sqrt{r_1^3/g}\partial\bar{G}/\partial z$$

are also readily obtained. In this case, $\mathscr{L} = 1/2$ in Eq. (24) and the B_i are tabulated in Table 1.

4.2. The impulsive wave height potential

Referring to Eq. (15) and setting $r_1 = \sqrt{x^2 + z^2}(\boldsymbol{\xi} = \mathbf{0})$ with

$$\lambda = \kappa r_1, \qquad \mu = \frac{-z}{r_1}, \qquad \tau = \sqrt{\frac{g}{r_1}}t,$$

gives

$$\phi_I(\mathbf{r}, \tau\sqrt{r_1/g}) = \frac{g}{2\pi}[F_1(\mu, -1, \tau) - F_2(\mu, -1, \tau)] \tag{29}$$

where F_1 corresponds to the $\sin(\sqrt{1-\mu^2}\lambda)\cos(\sqrt{\lambda}\tau)$ combination in Eq. (22) and F_2 to the $\cos(\sqrt{1-\mu^2}\lambda)\sin(\sqrt{\lambda}\tau)$ combination. Since F_1 and F_2 satisfy the ODE in Eq. (23) with the same coefficients given by Eq. (24) with $\mathscr{L} = -1$, so does $\bar{F} \triangleq F_1 - F_2$. The initial conditions for $\bar{F}$ can be obtained by evaluating the integral(s) and their time derivatives in Eq. (22) at $\tau = 0$. Evaluating the ensuing Laplace transforms gives

$$B_0 = \tan^{-1}\left[\frac{\sqrt{1-\mu^2}}{\mu}\right], \qquad B_1 = -\sqrt{\frac{\pi(1+\mu)}{2}},$$
$$B_2 = -\sqrt{1-\mu^2}, \qquad B_3 = -\sqrt{\frac{\pi(1+\mu)}{2}}\,\frac{1-2\mu}{2} \tag{30}$$

which must be multiplied by $g/(2\pi)$ to recover ϕ_I. The values of the B_i are also given in Table 1 for $(2\pi r_1/g)\partial\phi_I/\partial x$ and $(2\pi r_1/g)\partial\phi_I/\partial z$.

Note that the ODE in Eq. (23) can be integrated forward and backward in time from the initial conditions at $t = 0$ to produce the total solution. It will be used here to generate the causal part through forward integration and corresponds to multiplying ϕ_I in Eq. (15) by the Heaviside function $H(t)$. Since $\mathscr{L} = -1$, A_0 in Eq. (23) vanishes and therefore $\phi_I(\mathbf{r}, t) + C_I$ is also a solution which can be accommodated by adding the constant $(2\pi/g)C_I$ to the initial condition B_0 in Eq. (30). Since the physical quantities velocity and pressure depend only on the space and time derivatives of ϕ_I, it seems consistent that ϕ_I can be biased in this way. The value assigned to C_I will be discussed in the next section.

5. Rational approximation of the diffraction mapping

In Ref. [12], it was shown how rational approximations could be constructed for the Laplace transform $\tilde{F}(s) = \mathscr{L}\{F(\tau)\}$ when $F(\tau)$ is a solution of the time-varying ODE in Eq. (23) (the arguments $(\mu, \mathscr{L})$ are dropped in this section). We quickly review the procedure here since the initial conditions in Eq. (25) are more general than those used in Ref. [12]. Taking the Laplace transform of Eq. (23) and using the initial conditions in Eq. (25) yields an ODE in s for $\tilde{F}(s)$:

$$\gamma_2 s^2\tilde{F}''(s) + (\beta_3 s^3 + \beta_1 s)\tilde{F}'(s) + (\alpha_4 s^4 + \alpha_2 s^2 + \alpha_0)\tilde{F}(s) = \delta_3 s^3 + \delta_2 s^2 + \delta_1 s + \delta_0 \tag{31}$$

where

$$\gamma_2 = \bar{A}_2, \qquad \beta_1 = 4\bar{A}_2 - A_1, \qquad \beta_3 = -A_3,$$
$$\alpha_0 = A_0 - A_1 + 2\bar{A}_2,$$
$$\alpha_2 = A_2 - 3A_3, \qquad \alpha_4 = A_4,$$
$$\delta_0 = (A_2 - A_3)B_1 + A_4B_3, \quad \delta_1 = A_4B_2 + (A_2 - 2A_3)B_0,$$
$$\delta_2 = A_4B_1, \qquad \delta_3 = A_4B_0.$$

A rational approximation of $\tilde{F}(s)$ is required which is analytic in $Re\{s\} > 0$ corresponding to the causal nature of $F(\tau)$.

First, the problem is mapped into the complex z-plane using the bilinear transformation $s = (1-z)/(1+z)$ and its inverse $z = (1-s)/(1+s)$ which isomorphically maps the open right-half of the s-plane onto the open unit disk $|z| < 1$. Writing $\hat{F}(z) = \tilde{F}[(1-z)/(1+z)]$, and transforming Eq. (31) yields

$$\begin{aligned}\gamma_2(z-1)^2(z+1)^6\hat{F}''(z) &+ 2[\gamma_2(z-1)^2(z+1)^5 \\ &+ \beta_3(z-1)^3(z+1)^3 + \beta_1(z-1)(z+1)^5]\hat{F}'(z) \\ &+ 4[\alpha_4(z-1)^4 + \alpha_2(z-1)^2(z+1)^2 + \alpha_0(z+1)^4]\hat{F}(z) \\ &= -4[\delta_3(z-1)^3(z+1) - \delta_2(z-1)^2(z+1)^2 \\ &+ \delta_1(z-1)(z+1)^3 - \delta_0(z+1)^4]\end{aligned} \tag{32}$$

where $(\cdot)'$ now refers to differentiation with respect to z. If $\tilde{F}(s) \in \mathscr{H}_\infty$, then $\hat{F}(z)$ is a bounded analytic function in the unit disk [15] which permits a representation in terms of the uniformly convergent power series

$$\hat{F}(z) = \lim_{N\to\infty}\sum_{i=0}^{N} h_i z^i, \tag{33}$$

where the $\{h_i\}$ are known as the Hankel coefficients. Substituting this into Eq. (32) and matching powers of z yields an infinite system of linear equations for the $\{h_i\}$ which can be truncated at $N = 2n$.

A rational approximation to $\tilde{F}(s)$ can be obtained by letting $z = (1-s)/(1+s)$ in Eq. (33). State-space manipulations are presented by Damaren [12] which show

how to write $\tilde{F}(s)$ in the form

$$\tilde{F}(s) = \hat{F}\left(\frac{1-s}{1+s}\right) = \mathbf{c}^{\mathrm{T}}(s\mathbf{1} - \mathbf{A})^{-1}\mathbf{b} + d \tag{34}$$

with $\mathbf{A}$, $\mathbf{b}$, $\mathbf{c}$, and d being determined by the h_i. The major advantage of Eq. (34) lies in its time-domain realization. Let us identify $\tilde{\phi}_I(\mathbf{r}, s)$ with $\tilde{F}(s)$ which corresponds to the choice of coefficients in Eq. (24) with $\mathcal{L} = -1$ and the B_i in Eq. (30) multiplied by $g/(2\pi)$. Consider $\tilde{\Phi}_{\mathrm{I}}(\mathbf{r}, s) = \tilde{\phi}_{\mathrm{I}}(\mathbf{r}, s)\tilde{\zeta}_0(s)$, which mimics the Laplace transform of Eq. (16). Then,

$$\begin{aligned} \Phi_{\mathrm{I}}(\mathbf{r}, t) &= \int_0^t \phi_{\mathrm{I}}(\mathbf{r}, t-\tau)\zeta_0(\tau)\,\mathrm{d}\tau = \mathbf{c}^T\mathbf{x}(t) + d\zeta_0(t), \\ \dot{\mathbf{x}} &= \mathbf{A}\mathbf{x} + \mathbf{b}\zeta_0(t), \end{aligned} \tag{35}$$

which approximates the convolution in Eq. (16) for fixed $\mathbf{r}$. The validity of this can be established by taking Laplace transforms and recovering $\tilde{\Phi}_{\mathrm{I}}(\mathbf{r}, s) = \tilde{F}(s)\tilde{\zeta}_0(s)$ with $\tilde{F}(s)$ as given by Eq. (34). Note that $\phi_{\mathrm{I}}(\mathbf{r}, t) = \mathscr{L}^{-1}\{\tilde{F}(s)\}$ is the impulse response, i.e. $\Phi_{\mathrm{I}}(\mathbf{r}, t) = \phi_{\mathrm{I}}(\mathbf{r}, t)$ when $\zeta_0(t) = \delta(t)$ which can also be obtained by solving $\dot{\mathbf{x}} = \mathbf{A}\mathbf{x}$ ($\delta_0(t) = 0$) with $\mathbf{x}(0) = \mathbf{b}$ leading to

$$\phi_{\mathrm{I}}(\mathbf{r}, t) = \mathbf{c}^{\mathrm{T}} \exp(\mathbf{A}t)\mathbf{b}\cdot H(t). \tag{36}$$

Here, we have taken $d = 0$ since $d = \lim_{s\to\infty}\tilde{F}(s)$ which should vanish when one considers Eq. (13) as $\omega \to \infty$.

5.1. State-space representation of the Froude–Krylov force

The exciting force acting on the body in mode α (Froude–Krylov part) is

$$f_{\mathrm{I}\alpha}(t) = \rho\frac{\partial}{\partial t}\int_S \Phi_{\mathrm{I}}(\mathbf{r}, t)n_\alpha\,\mathrm{d}S$$

and its Laplace transform satisfies

$$f_{\mathrm{I}\alpha}(s) = \left[\rho s\int_S \tilde{\phi}_{\mathrm{I}}(\mathbf{r}, s)n_\alpha\,\mathrm{d}S\right]\tilde{\zeta}_0(s). \tag{37}$$

Describing $\tilde{\phi}_I(\mathbf{r}, s)$ according to Eqs. (33) and (34) yields

$$\begin{aligned} \rho\int_S \tilde{\phi}_{\mathrm{I}}(\mathbf{r}, s)n_\alpha(\mathbf{r})\,\mathrm{d}S &= \lim_{N\to\infty}\rho\int_S \sum_{i=0}^{N} h_i(\mathbf{r})\left[\frac{1-s}{1+s}\right]^i n_\alpha(\mathbf{r})\,\mathrm{d}S \\ &= \lim_{N\to\infty}\sum_{i=1}^{N}\left[\rho\int_s h_i(\mathbf{r})n_\alpha(\mathbf{r})\,\mathrm{d}S\right]\left[\frac{1-s}{1+s}\right]^i \\ &= \lim_{N\to\infty}\sum_{i=0}^{N} H_i z^i,\quad H_i = \rho\int_S h_i(\mathbf{r})n_\alpha(\mathbf{r})\,\mathrm{d}\mathbf{S}, \end{aligned} \tag{38}$$

for the causal approximation to $s^{-1}\tilde{H}_{\mathrm{I}\alpha}(s)$.

As suggested in Ref. [12], the spatial integration in Eq. (38) can be evaluated using Gauss–Legendre quadrature where the parameters $\{h_i\}$ are evaluated for a discrete set of points on S, $\mathbf{r} = \mathbf{r}_j$, and the integration performed as a weighted sum of the h_i evaluated at these points thus yielding the effective parameters $\{H_i\}$. Effective matrices $(\mathbf{A}_e, \mathbf{b}_e, \mathbf{c}_e)$ corresponding to the operations alluded to in Eq. (34) can then be constructed. With this representation in hand, the Froude–Krylov force corresponding to the inverse Laplace transform of Eq. (37) is

$$\begin{aligned} f_{\mathrm{I}\alpha}(t) &= \dot{y}, \qquad y = \mathbf{c}_e^{\mathrm{T}}\mathbf{x}, \\ \dot{\mathbf{x}} &= \mathbf{A}_e\mathbf{x} + \mathbf{b}_e\zeta_0(t) = \mathbf{c}_e^{\mathrm{T}}\mathbf{A}_e\mathbf{x}(t) + \mathbf{c}_e^{\mathrm{T}}\mathbf{b}_e\zeta_0(t) \end{aligned} \tag{39}$$

which can be identified with the form in Eqs. (18) and (19) if

$$\mathbf{A}_{\mathrm{I}} = \mathbf{A}_e, \qquad \mathbf{B}_{\mathrm{I}} = \mathbf{b}_e, \qquad \mathbf{C}_{\mathrm{I}} = \mathbf{c}_e^{\mathrm{T}}\mathbf{A}_e, \qquad \mathbf{D}_{\mathrm{I}} = \mathbf{c}_e^{\mathrm{T}}\mathbf{b}_e. \tag{40}$$

Using the final value theorem for Laplace transforms in conjunction with Eq. (34) for $\tilde{\phi}_{\mathrm{I}}(\mathbf{r}, s)$ we have

$$\lim_{t\to 0}\phi_{\mathrm{I}}(\mathbf{r}, t) = \lim_{s\to\infty} s\tilde{\phi}_{\mathrm{I}}(\mathbf{r}, \mathbf{s}) = \lim_{s\to\infty} s\mathbf{c}^{\mathrm{T}}(s\mathbf{1} - \mathbf{A})^{-1}\mathbf{b} = \mathbf{c}^{\mathrm{T}}\mathbf{b}.$$

Note that $\partial\phi_{\mathrm{I}}/\partial t$ calculated using Eq. (36) will contain the Dirac delta function if $\mathbf{c}^{\mathrm{T}}\mathbf{b} \neq 0$. For this reason, C_{I} discussed at the end of Section 4 is selected to be $C_{\mathrm{I}} = -gB_0|_{\mu=0}/(2\pi) = -g/4$ so that for $\mathbf{r} \in F$ (i.e. $\mu = 0$), $\mathbf{c}^{\mathrm{T}}\mathbf{b} = \phi_{\mathrm{I}}(\mathbf{r}, 0) = 0$. A physical interpretation of this value is possible. Integrating Eq. (14) and taking $\Phi_{\mathrm{I}}(\mathbf{r}, t) = 0$, $t < 0$, gives

$$\Phi_{\mathrm{I}}(\mathbf{r}, 0) = -g\int_{-\infty}^{0}\zeta_{\mathrm{I}}(x, y, t)\,\mathrm{d}t, \qquad \mathbf{r} \in F. \tag{41}$$

In adopting a causal approximation for $\Phi_{\mathrm{I}}(\mathbf{r}, t)$, we argue that the entire function should be shifted so that $\Phi_{\mathrm{I}}(\mathbf{r}, 0) = 0$, $\mathbf{r} \in F$. From Eq. (41), this is consistent with neglecting the past history of the incident waves. However, physically, having destroyed the past history of the waves (and introduced a step function $H(t)$ into $\Phi_{\mathrm{I}}(\mathbf{r},\mathrm{t})$), we have incurred an initial impulsive distribution of pressure on the free surface ($-\rho\partial\Phi_{\mathrm{I}}(\mathbf{0}, t)/\partial t$) which should also be removed. In summary, by resetting $B_0 = \tan^{-1}[\sqrt{1-\mu^2}/\mu] - \pi/2$, we obtain $\Phi_{\mathrm{I}}(\mathbf{r}, 0) = \phi_{\mathrm{I}}(\mathbf{r}, 0) = 0$ on the free surface ($\mathbf{r} \neq \mathbf{0}$) and hence $\partial\phi_{\mathrm{I}}/\partial t$ does not contain $\delta(t)$ for $\zeta_0(t) = \delta(t)$.

6. Numerical examples

In this section, the position is selected according to

$$\mathbf{r}^{\mathrm{T}} = a\left[\sqrt{1-\mu^2}\;0\;-\mu\right]^{\mathrm{T}}, \qquad \mu = -z/\sqrt{x^2+z^2}. \tag{42}$$

We are initially interested in comparing the exact frequency-domain description for the potential function in Eq. (13) with that generated by the rational approximation $\tilde{F}(j\hat{\omega}) = \mathbf{c}^{\mathrm{T}}(j\hat{\omega}\mathbf{1} - \mathbf{A})^{-1}\mathbf{b}$ ($\hat{\omega} = \sqrt{ka}$) in Eq. (34). Here, the value of $n = 15$ and the requirement that $\tilde{\phi}_{\mathrm{I}}(\mathbf{r}, s)$ be analytic for $\mathrm{Re}\{s\} > 0$ is equivalent to $\mathbf{A}$ having eigenvalues with negative real parts. The approach for removing extraneous eigenvalues with positive real parts is discussed in Ref. [12]. The value of n reflects this removal. On the basis of Eq. (13),

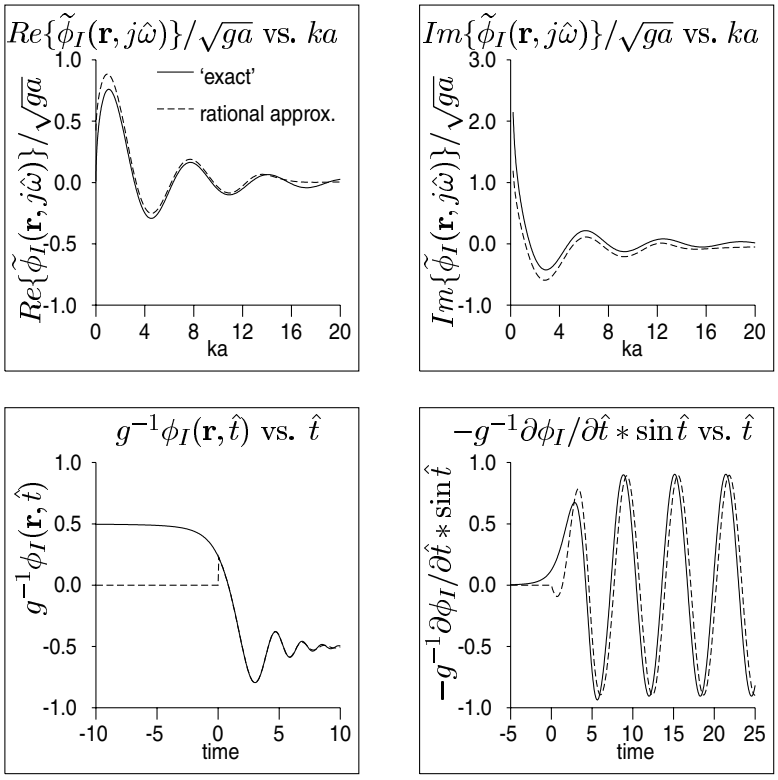

Fig. 1. Rational approximation of $\tilde{\phi}_1$ vs. exact solution ($\mu = 0.1,\ C_I = 0$).

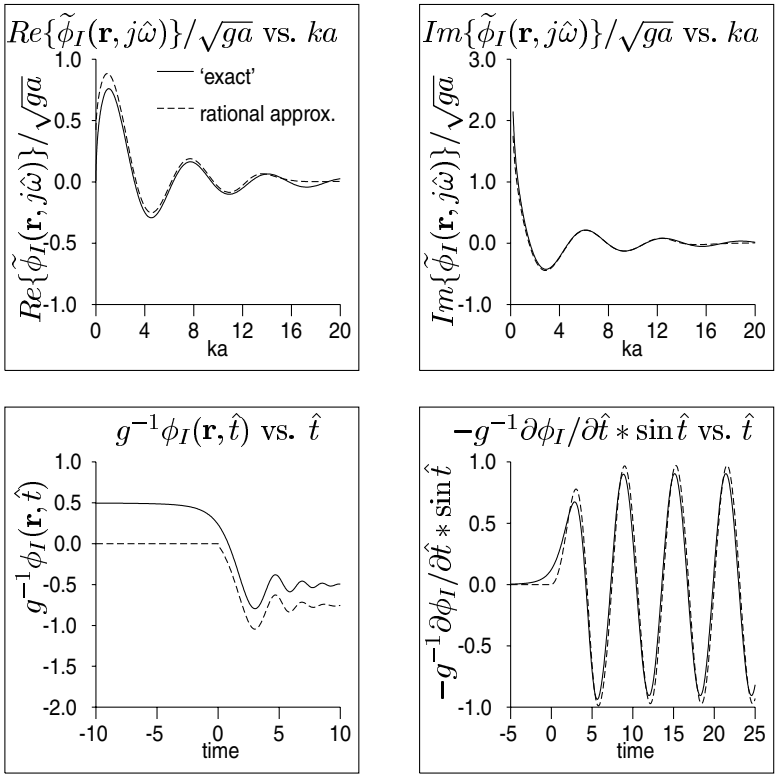

Fig. 2. Rational approximation of $\tilde{\phi}_1$ vs. exact solution ($\mu = 0.1,\ C_I = -g/4$).

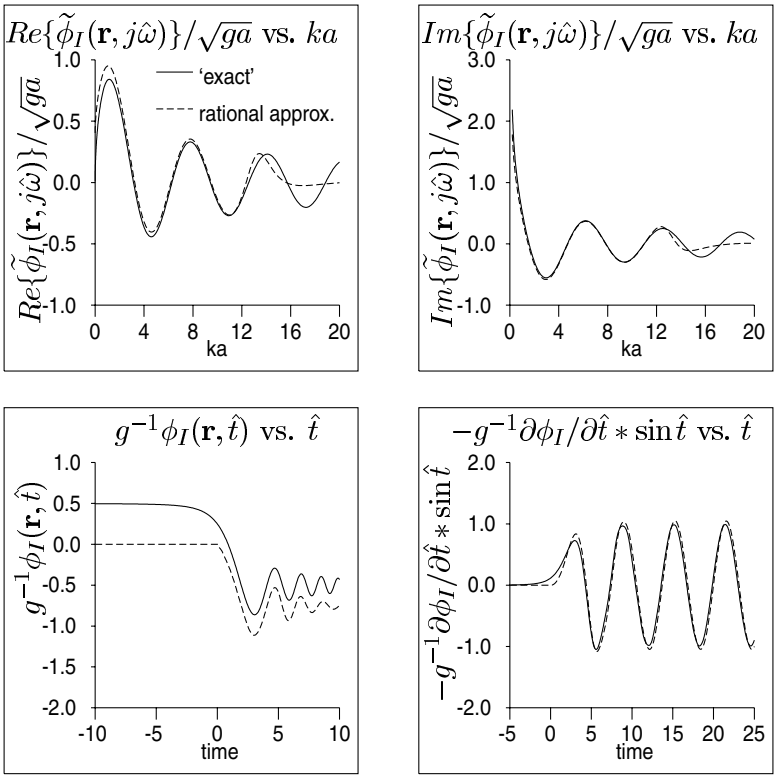

Fig. 3. Rational approximation of $\tilde{\phi}_I$ vs. exact solution ($\mu = 0.5,\ C_I = -g/4$).

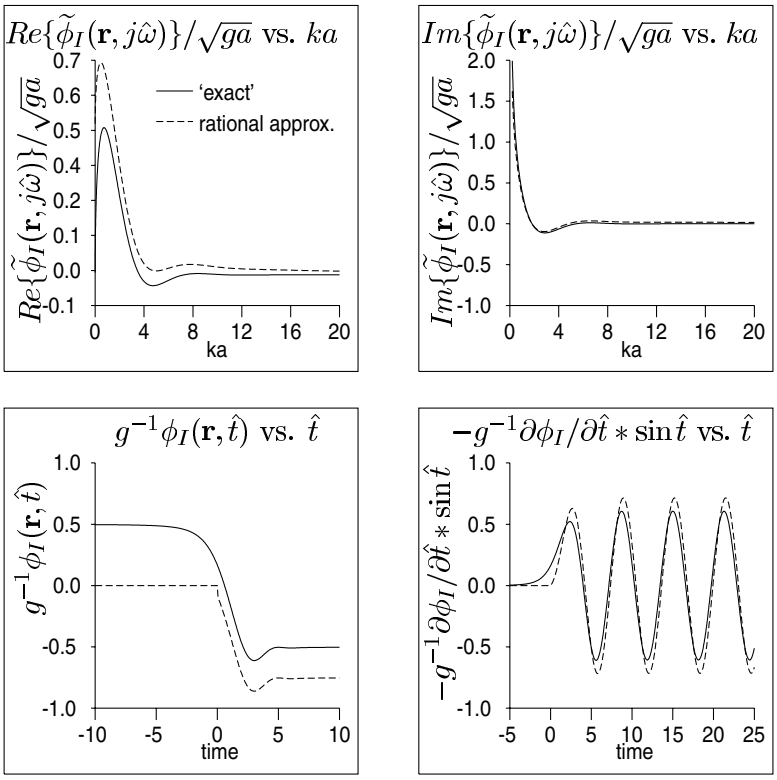

Fig. 4. Rational approximation of $\tilde{\phi}_I$ vs. exact solution ($\mu = 0.01,\ C_I = -g/4$).

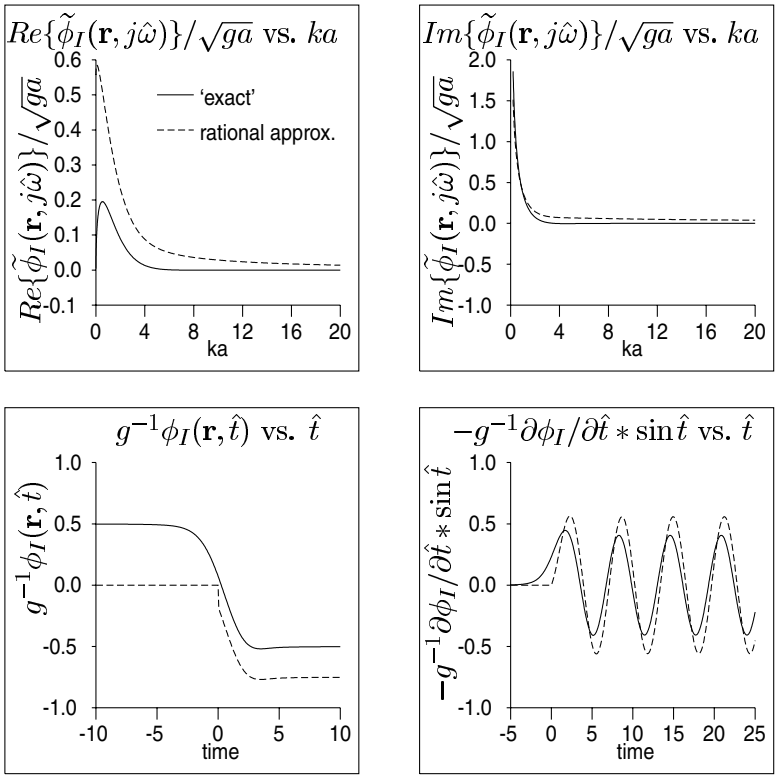

Fig. 5. Rational approximation of $\tilde{\phi}_I$ vs. exact solution ($\mu = 0.9$, $C_I = -g/4$).

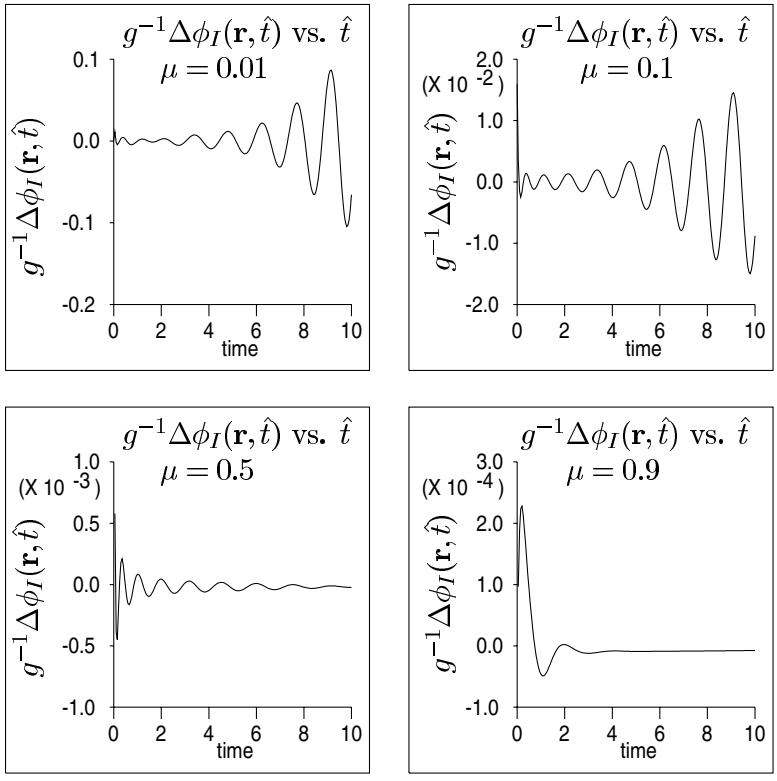

Fig. 6. Errors in rational approximation for $\tilde{\phi}_I$ for various μ ($C_I = 0$).

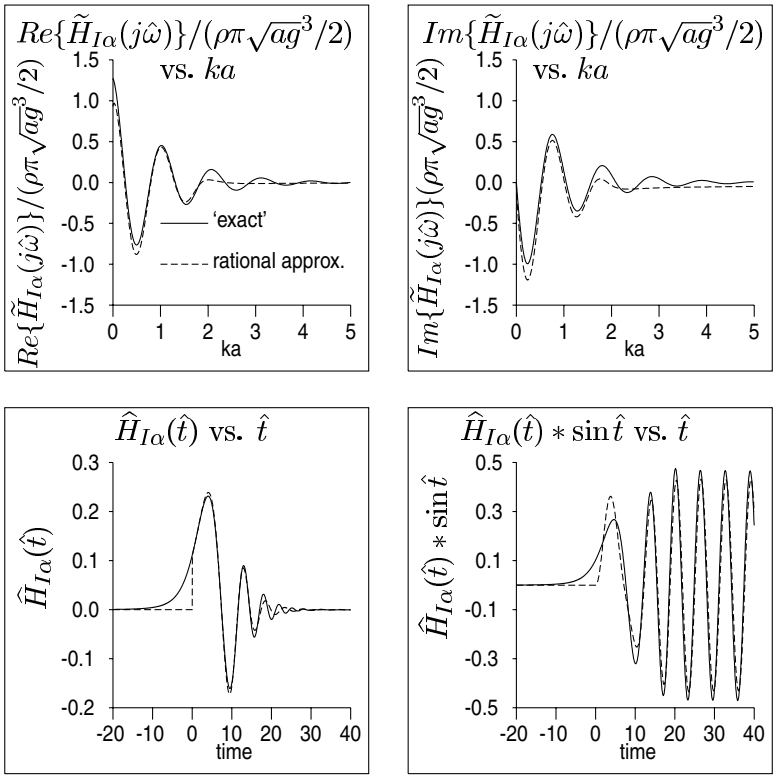

Fig. 7. Rational approximation of the Froude–Krylov (heave) force for a circular cylinder [$H_{I\alpha} = (\rho\pi ag/2)\hat{H}_{I\alpha}$].

one expects $\tilde{F}(s)$ to have a pole at the origin and this consistently manifested itself in the rational approximation by an eigenvalue of $\mathbf{A}$ near $s = -10^{-6}$.

The corresponding time-domain functions $\phi_I(\mathbf{r},\hat{t})$ (with $\hat{t} = t\sqrt{g/a}$) are generated according to Eq. (15) using the trapezoidal rule and the causal approximation using Eq. (36). It is the time derivative of the incident potential that is used to derive the Froude–Krylov force and the height of the incident wave on the free surface according to Eq. (14). For this reason, we look at the solution for $-g^{-1}\partial\Phi_I(\mathbf{r},\hat{t})/\partial\hat{t}$ corresponding to $\zeta_0(\hat{t}) = [\sin\hat{t}\,]H(\hat{t})$. The exact solution is calculated by differentiating Eq. (16) to get

$$\frac{\partial\Phi_I(\mathbf{r},\hat{t})}{\partial\hat{t}} = \int_0^\infty \frac{\partial\phi_I(\mathbf{r},\hat{t}-\tau)}{\partial\hat{t}}\zeta_0(\tau)\,\mathrm{d}\tau$$

For the rational approximation, the corresponding time function is obtained from the derivative of Eq. (35), $\partial\Phi_I(\hat{t})/\partial\hat{t} = \mathbf{c}^T\mathbf{A}\mathbf{x}(\hat{t}) + \mathbf{c}^T\mathbf{b}\delta_0(\hat{t})$ where $\mathbf{x}(\hat{t})$ was obtained by integrating Eq. (35) using a fourth-order Runge–Kutta technique with a step-size of $\Delta\hat{t} = 0.05$.

The results of these calculations are presented in Fig. 1 for $\mu = 0.1$, where initially $C_I = 0$. The causal portions of the time-domain potential exhibit excellent agreement and in the frequency domain, the discrepancy can be largely attributed to the Fourier transform of the missing anticausal part. This is approximately given by $g^{-1}\phi_I(\mathbf{r},\hat{t}) = (1/2)H(-\hat{t})$ or $(1/2)j/\hat{\omega}$ in the frequency domain (in any event, the time-domain behavior as $t \to \pm\infty$ dictates that in the frequency domain as $s \to 0$). The convolution which illustrates the evolution of the pressure distribution (within a factor of ρg) at $\mu = 0.1$ clearly illustrates the noncausality of the 'exact' case and the approximation clearly possesses a delay.

The situation when $C_I = -g/4$ is depicted in Fig. 2. The resulting bias in the time-domain eliminates much of the discontinuity in $\phi_I(\mathbf{r},0)$ (all of it is eliminated on the free surface, i.e. as $\mu \to 0$; see Fig. 3). The resulting addition of $-jC_I/\hat{\omega}$ in the frequency domain greatly improves the accuracy of the imaginary part of the causal approximation. The delay in the convolution with the unit frequency sinusoid is largely mitigated and in the steady-state there is fairly good agreement. The corresponding graphs for $\mu = 0.01$, $\mu = 0.5$, and $\mu = 0.9$ are shown in Figs. 3–5. Note that on the free surface ($\mu \to 0$ which is approximated in Fig. 3), the convolution in the lower right corner corresponds to the time evolution of the free surface elevation corresponding to an impressed sinusoid at the origin. A slight delay in its buildup is in evidence as well as a small steady-state amplitude error. The latter is in accord with the frequency domain discrepancy at $ka = 1$; both effects are produced by causalization of the approximation. As $\mu \to 1$, the accuracy of the rational approximation decreases in the frequency domain but the effective contribution to the Froude–Krylov force also decreases.

The discrepancy between the two sets of curves in Figs. 2–5 can be attributed to three factors: (i) the shift by C_I in the time domain; (ii) truncating the anticausal part of ϕ_I (i.e. setting $\phi_I(\mathbf{r},t) = 0$, $t < 0$; (iii) truncating the order of

the rational approximation and hence the order of the state-space system at n states. It has already been observed that the effect of (i) largely offsets that of (ii) when considering the imaginary part in the frequency domain. In order to assess (iii) alone as a function of μ, we compare the causal part of

$$g^{-1}\Delta\phi(\mathbf{r},\hat{t}) = g^{-1}[\phi(\mathbf{r},\hat{t})|_{\text{approx}} - \phi(\mathbf{r},\hat{t})|_{\text{exact}}]$$

where the C_I factor is neglected in calculating the difference. The behavior of this quantity is shown in Fig. 6 for various values of μ. The accuracy of the rational approximation in the time domain (for fixed n) improves as $\mu \to 1$.

In determining the Froude–Krylov force it is a weighted spatial superposition of $\partial\phi_I(\mathbf{r},t)/\partial t$ that is required or $j\omega\tilde{\phi}_I(\mathbf{r}, j\omega)$ in the frequency domain. This tends to mitigate low-frequency errors and accentuate higher frequency ones. On this basis, one expects the methodology to perform better at larger draughts which is consistent with the results of Ref. [12] for the radiation problem.

The determination of the transient exciting force on a circular cylinder of radius a and draft a is considered with its center located at $x = 6a$, $z = 0$ Eq. (15). The 'exact' calculation in the frequency domain uses a weighted version of Eq. (13) in conjunction with Eq. (17). The spatial integrals are performed using a 48-point Gauss–Legendre rule. The time-domain solutions were obtained by calculating a numerical inverse Fourier transform in Eq. (17) and performing the convolution in Eq. (21) using the trapezoidal rule. The rational approximations were obtained by applying the 48-point rule to Eq. (38). The convolution with the sinusoidal wave height was accomplished through numerical integration of the effective system in Eqs. (18) and (19). The results are shown in Fig. 7. The rational approximation captures the small-time behavior of the causal part of the impulse response quite well. The convolution exhibits an initial transient error relative to the 'exact' noncausal solution but in the steady-state, the increment is quite accurate. It is interesting to note that the noncausal nature of the exact solution persists in spite of the shifting of the wave-height datum six cylinder radii up-wave of the body center.

7. The transient Haskind relations

The transient form of the Haskind Relations [11] states that

$$f_{D\alpha}(t) = \rho\int_{-\infty}^{t}\int_S\left[\frac{\partial\Phi_I}{\partial t}(\mathbf{r},\tau)\frac{\partial\phi_{R\alpha}}{\partial n}(\mathbf{r},t-\tau) - \frac{\partial^2\Phi_I}{\partial n\partial t}(\mathbf{r},\tau)\phi_{R\alpha}(\mathbf{r},t-\tau)\right]\mathrm{d}S\,\mathrm{d}\tau \tag{43}$$

where $\phi_{R\alpha}$, from Eq. (7), is the radiation potential due to an impulsive velocity motion in mode α. This can be interpreted as the inverse Fourier transform of the steady-state relations which are given by

$$\tilde{f}_{D\alpha}(j\omega) = \left\{j\omega\rho\int_S\left[\tilde{\phi}_I(\mathbf{r},j\omega)\frac{\partial\tilde{\phi}_{R\alpha}}{\partial n}(\mathbf{r},j\omega) - \frac{\partial\tilde{\phi}_I}{\partial n}(\mathbf{r},j\omega)\tilde{\phi}_{R\alpha}(\mathbf{r},j\omega)\right]\mathrm{d}S\right\}\tilde{\zeta}_0(j\omega). \tag{44}$$

Making use of the boundary condition in Eq. (7), allows us to identify the first term in Eq. (43) with Eq. (8) and the first term in Eq. (44) with Eq. (17). Using the remaining terms, the scattered portion of the diffraction force can be written as

$$\tilde{f}_{S\alpha} = \tilde{H}_{S\alpha}(j\omega)\tilde{\zeta}_0,$$
$$\tilde{H}_{S\alpha}(j\omega) =\triangleq -j\omega\rho\int_S\left(\frac{\partial\tilde{\phi}_I}{\partial n}\tilde{\phi}_{R\alpha}\right)\mathrm{d}S. \tag{45}$$

We seek to realize the mapping from $\zeta_0(t)$ to $f_{S\alpha}(t)$ along the lines of Eqs. (18) and (19).

Note that $\partial\phi_I(\mathbf{r},t)/\partial n = \mathbf{n}^T(\mathbf{r})\nabla\phi_I$ where $\partial\phi_I/\partial x$ and $\partial\phi_I/\partial z$ can be determined as solutions of Eq. (23) with $\mathcal{L} = 0$. By weighting the initial conditions in Table 1 using the components of the normal, it is possible to realize $\partial\tilde{\phi}_I/\partial n$ in the form

$$\frac{\partial\hat{\phi}_I}{\partial n}(\mathbf{r},z) = \sum_{i=0}^{\infty}h_{Ii}(\mathbf{r})z^i.$$

Assuming a similar series for $\hat{\phi}_{R\alpha}(\mathbf{r},z)$ can be developed based on the results in Ref. [12] (with coefficients h_{Ri}), the product in the integrand of Eq. (45) can be written as

$$-\frac{\partial\tilde{\phi}_I}{\partial n}\tilde{\phi}_{R\alpha}(\mathbf{r},s) = -\left[\sum_{i=0}^{\infty}h_{Ii}(\mathbf{r})z^i\right]\left[\sum_{i=0}^{\infty}h_{Ri}(\mathbf{r})z^i\right]_{z=(s-1)/(s+1)} = \sum_{i=0}^{\infty}H_{RI,i}\left[\frac{s-1}{s+1}\right]^i$$

where the $H_{RI,i}$ are determined by multiplying the two series. This can be realized in the form of Eq. (34) and the output $f_{S\alpha}(t)$ can then be determined in a similar manner to $f_{I\alpha}(t)$ in Eqs. (39) and (40) where the effective matrices ($\mathbf{A}_e$, $\mathbf{b}_e$, $\mathbf{c}_e$) are chosen so that

$$\mathbf{c}_e^T(s\mathbf{1}-\mathbf{A})^{-1}\mathbf{b}_e = \sum_{i=0}^{\infty}\rho\int_S H_{RI,i}(\mathbf{r})\,\mathrm{d}S\left[\frac{s-1}{s+1}\right]^i.$$

Another possibility is to realize that Eq. (44) also applies when the integral is performed around a bounding surface, S_∞, which encloses the body (after multiplication by -1) which follows from applying Green's theorem. By choosing S_∞ to be a cylinder of large radius, an asymptotic expression for $\tilde{\phi}_{R\alpha}$ can be used. In 2D problems with left–right symmetric motions, $\tilde{\phi}_{R\alpha} \propto \tilde{\mathcal{G}}(\mathbf{r},\mathbf{0};j\omega)$ in Eq. (26) and hence the coefficients h_{Ri} can be determined using the techniques of Section 5.

8. Concluding remarks

This paper has been motivated by the requirement of modeling the transient relationship between an incident sea state and the exciting forces on a floating body. It has been observed that this mapping is noncausal since the forces acting the body arise before the datum wave height is "turned on." Since this is problematic in a simulation environment, we have endeavored to develop an (optimal) causal approximation.

Although an initial transient error exists relative to the noncausal solution, the steady-state accuracy for sufficiently low frequencies is quite good. Since the diffraction mapping is linear time-invariant, it can be realized as a nonhomogeneous system of first-order constant-coefficient ODEs with the wave height datum as the forcing function. These are highly amenable to computer implementation of the simulation problem. The ODEs were developed using an analytical approach to constructing rational approximations for the diffraction mapping in the frequency domain. This was accomplished using the fourth-order time-varying ODE which the 2D Green's functions relative to an impulsive source and an impulsive wave height were shown to satisfy.

The realization of the diffraction mapping can be readily combined with similar models for the floating body dynamics (forces to body motion mapping) and the radiation impedance (body velocities to radiation forces mapping). Future work will address the combination of these elements using the variational principle described in Ref. [12] in conjunction with the finite element method for capturing complex ship geometries in two dimensions. It is anticipated that this can form the basis for a computationally efficient "transient strip theory."

Appendix A. Proof of Lemma

Since many steps in the proof are common to that in Ref. [13] for the 3D source function, we emphasize the differences. In the original proof, a key observation was that the Bessel function of zeroth order could be expressed as $J_0(z) = \exp(-jz)M[1/2, 1, 2jz]$ where M is the confluent hypergeometric function (or Kummer's function) [16]. The analogous result used here is that

$$\cos z = z\exp(jz)M[1, 2, -2jz]. \tag{46}$$

Only the case with $\cos\sqrt{1-\mu^2}\lambda\,\sin\sqrt{\lambda}\tau$ in the integrand is treated. The other three possibilities can be handled similarly since $\sin z = z\exp(jz)M[1, 2, -2jz]$ also.

Begin by noting that Eq. (22) implies

$$\frac{\partial^{2k}F}{\partial\tau^{2k}} = (-1)^k\int_0^\infty \lambda^{\ell+k}\mathrm{e}^{-\mu\lambda}\cos\sqrt{1-\mu^2}\lambda\,\sin\sqrt{\lambda}\tau\,\mathrm{d}\lambda,$$

$k = 0, 1, 2, \ldots,$

and making the change of variable $p = \lambda\tau^2$ gives

$$\frac{\partial^{2k}F}{\partial\tau^{2k}} = \frac{(-1)^k}{\tau^{2(\ell+k+1)}}\int_0^\infty \mathrm{e}^{-p\mu/\tau^2}\cos\left(p\sqrt{1-\mu^2}/\tau^2\right)p^{\ell+k}\sin\sqrt{p}\,\mathrm{d}p.$$

Introducing the new variable $u = 1/\tau^2$ leads to

$$F = \int_0^\infty u^{\ell+1}\mathrm{e}^{-pu\mu}\cos\left(pu\sqrt{1-\mu^2}\right)p^{\ell}\,\sin\sqrt{p}\,\mathrm{d}p.$$

Using the relationship in Eq. (46) and defining

$$\alpha(\mu) = \sqrt{1-\mu^2},$$

$$H_\ell(p,\mu,u) = u^{\ell+2}\exp[-pu(\mu + j\alpha(u))]$$

$$\times M([1, 2, -2jpu\alpha(\mu)] = u^{-A}\mathrm{e}^{-f(u)}M[a, b, h(u)] \tag{47}$$

where $A = -(\ell + 2)$, $f(u) = up(\mu + j\alpha(\mu))$, $a = 1$, $b = 1$, and $h(u) = -2jup\alpha(\mu)$, leads to

$$F = \alpha(\mu)\int_0^\infty H_\ell(p,\mu,u)p^{\ell+1}\sin\sqrt{p}\,\mathrm{d}p, \tag{48}$$

$$(-1)^k\tau^{2k}\frac{\partial^{2k}F}{\partial\tau^{2k}} = \alpha(\mu)\int_0^\infty H_\ell(p,\mu,u)p^{\ell+k+1}\sin\sqrt{p}\,\mathrm{d}p, \tag{49}$$

$k = 1, 2, 3, \ldots.$

The function H defined this way is known to satisfy the general confluent equation (see Eq. (3.11) in [13] or [25, 13.1.35, pp. 505] in [16]) which in the present case takes the form

$$\frac{\partial^2 H_\ell}{\partial u^2} - \left[2(\ell+1) - \frac{2\mu pu}{u}\right]\frac{\partial H_\ell}{\partial u}$$

$$+\left[p^2 - \frac{2p\mu(\ell+1)}{u} + \frac{\ell^2+3\ell+2}{u^2}\right]H_\ell = 0.$$

Letting

$$u = \frac{1}{\tau^2}, \qquad \frac{\partial}{\partial u} = -\frac{1}{2}\tau^3\frac{\partial}{\partial\tau},$$

$$\frac{\partial^2}{\partial u^2} = \frac{3}{4}\tau^5\frac{\partial}{\partial\tau} + \frac{1}{4}\tau^6\frac{\partial^2}{\partial\tau^2}$$

this becomes

$$\frac{1}{4}\tau^6\frac{\partial^2 H_\ell}{\partial\tau^2} + \left(\ell + \frac{7}{4}\right)\tau^5\frac{\partial H_\ell}{\partial\tau} + (\ell+1)(\ell+2)\tau^4 H_\ell$$

$$= p\mu\tau^3\frac{\partial H_\ell}{\partial\tau} - p^2 H_\ell + 2p\mu(\ell+1)\tau^2 H_\ell. \tag{50}$$

Now multiply both sides by $\alpha(\mu)p^{\ell+1}\sin\sqrt{p}$ and integrate with respect to p from 0 to ∞. Using Eqs. (48) and (49), we note the appearance of F and its derivatives on the left-hand

side of Eq. (50) so that it becomes:

$$\frac{1}{4}\tau^6\frac{\partial^2 F}{\partial\tau^2}+\left(\ell+\frac{7}{4}\right)\tau^5\frac{\partial F}{\partial\tau}+(\ell+1)(\ell+2)\tau^4 F$$
$$=\mu\tau^3\frac{\partial}{\partial\tau}\int_0^\infty \alpha(\mu)H_\ell(p,\mu,u)p^{\ell+2}\sin\sqrt{p}\,\mathrm{d}p$$
$$-\int_0^\infty \alpha(\mu)H_\ell(p,\mu,u)p^{\ell+3}\sin\sqrt{p}\,\mathrm{d}p$$
$$+2\mu\tau^2(\ell+1)\int_0^\infty \alpha(\mu)H_\ell(p,\mu,u)p^{\ell+2}\sin\sqrt{p}\,\mathrm{d}p.$$

The integrals on the right-hand side are available from Eq. (49) which leads to Eq. (23) after simplification. □

References

[1] Cummins WE. The impulse response function and ship motions. Schiffstechnik 1962;9:101–9.

[2] Wehausen JV. Initial-value problem for the motion in an undulating sea of a body with fixed equilibrium position. Journal of Engineering Mathematics 1967;1(1):1–17.

[3] Yu Z, Falnes J. State-space modelling of a vertical cylinder in heave. Applied Ocean Research 1995;17:265–75.

[4] Falnes J. On non-causal impulse response functions related to propagating water waves. Applied Ocean Research 1995;17:379–89.

[5] Damaren CJ. Time-domain floating body dynamics by rational approximation of the radiation impedance and diffraction mapping. Ocean Engineering 1999;27(6):687–705.

[6] Yeung RW. The transient heaving motion of floating cylinders. Journal of Engineering Mathematics 1982;16:97–119.

[7] Newman JN. Transient axisymmetric motion of a floating cylinder. Journal of Fluid Mechanics 1985;157:17–33.

[8] Beck RF, Liapis S. Transient motions of floating bodies at zero forward speed. Journal of Ship Research 1987;31(3):164–76.

[9] Pot G, Jami A. Some numerical results in 3-D transient linear naval hydrodynamics. Journal of Ship Research 1991;35(4):295–303.

[10] Beck RF. Time-domain computations for floating bodies. Applied Ocean Research 1994;16:267–82.

[11] Korsmeyer FT, Bingham HB. The forward speed diffraction problem. Journal of Ship Research 1998;42(2):99–112.

[12] Damaren CJ. Transient free-surface hydrodynamics using rational approximation of the Green's function. Journal of Ship Research 1999;43(2):95–106.

[13] Clément AH. An ordinary differential equation for the Green function of time-domain free-surface hydrodynamics. Journal of Engineering Mathematics 1998;33(2):201–17.

[14] Thorne RC. Multipole expansions in the theory of surface waves. Proceedings of the Cambridge Philosophical Society 1953;49:707–16.

[15] Hoffman K. Banach spaces of analytic functions. New York: Dover Publications, 1962.

[16] Abramowitz M, Stegun IA. Handbook of mathematical functions. New York: Dover Publications, 1965.